# Surface functionalization of few-layer graphene on β -SiC(001) by Neutral Red dye

**Article** *in* Applied Surface Science · January 2022

DOI: 10.1016/j.apsusc.2022.152542



**17 authors**, including:

Dmitrii Potorochin
Technische Universität Bergakademie Freiberg
**14** PUBLICATIONS **81** CITATIONS
SEE PROFILE

Olga Molodtsova
Deutsches Elektronen-Synchrotron
**55** PUBLICATIONS **1,065** CITATIONS
SEE PROFILE

Victor Aristov
Institute of Solid State Physics RAS
**144** PUBLICATIONS **2,769** CITATIONS
SEE PROFILE

D. Marchenko
Helmholtz-Zentrum Berlin
**84** PUBLICATIONS **4,046** CITATIONS
SEE PROFILE

# Surface functionalization of few-layer graphene on $\beta$-SiC(001) by Neutral Red dye

Dmitrii V. Potorochin[a,b,c,d,*], Alexander N. Chaika[e,f], Olga V. Molodtsova[b,d], Victor Yu. Aristov[d,e,g], Dmitry E. Marchenko[h], Dmitry A. Smirnov[i], Anna A. Makarova[j], Brian Walls[f], Kuanysh Zhussupbekov[f,**], Killian Walshe[f], Igor V. Shvets[f], Anca S. Ciobanu[d], Maxim K. Rabchinskii[k], Nikolai V. Ulin[k], Marina V. Baidakova[b,k], Pavel N. Brunkov[b,k], Serguei L. Molodtsov[a,b,c]

[a] *European XFEL GmbH, Holzkoppel 4, Schenefeld, D-22869, Germany*
[b] *ITMO University, Kronverksky prospekt 49, Saint Petersburg, 197101, Russia*
[c] *Institute of Experimental Physics, TU Bergakademie Freiberg, Leipziger Straße 23, Freiberg, D-09599, Germany*
[d] *Deutsches Elektronen-Synchrotron DESY, Notkestrasse 85, Hamburg, D-22607, Germany*
[e] *Institute of Solid State Physics of the Russian Academy of Sciences, 2 Academician Ossipyan Street, Moscow District, 142432, Russia*
[f] *CRANN, School of Physics, Trinity College Dublin, Dublin 2, Ireland*
[g] *Institut für Theoretische Physik, Universität Hamburg, Luruper Chaussee 149, Hamburg, D-22761, Germany*
[h] *Helmholtz-Zentrum Berlin für Materialien und Energie, Albert-Einstein-Straße 15, Berlin, D-12489, Germany*
[i] *Institute of Solid State and Materials Physics, Dresden University of Technology, Dresden, D-01062, Germany*
[j] *Physical Chemistry, Institute of Chemistry and Biochemistry, Free University of Berlin, Arnimallee 22, Berlin, D-14195, Germany*
[k] *Ioffe Institute, Politekhnicheskaya 26, Saint Petersbur, 194021, Russia*

**Abstract**

Few-layer graphene on $\beta$-SiC(001) functionalized with phenazine dye Neutral Red by means of diazonium chemistry has been studied using X-ray photoelectron spectroscopy, near-edge X-ray absorption fine structure, photoemission electron microscopy, scanning tunneling microscopy, and density functional theory calculations. The experimental data reveal the formation of a composite phenazine dye/graphene structure with a large energy gap. The molecules in this structure can be oriented both parallel and perpendicular to the graphene surface. According to scanning tunneling spectroscopy and theoretical calculations, the density of electron states in different surface areas depends on the local short-range order and the molecules' environment. On the other hand, the photoemission spectroscopy study shows that the bottom layers of the few-layer graphene remain intact, which inherently makes the synthesized layered composite a low-dimensional metal/semiconductor heterostructure. In addition, photoemission electron microscopy imaging shows a high homogeneity of the dye-modified graphene on a micrometer scale.

*Keywords:* graphene, functionalization, organic dye, Neutral Red, XPS, NEXAFS, STM

## 1. Introduction

Graphene, a two-dimensional crystal consisting of carbon atoms arranged in a hexagonal lattice, has attracted special attention due to its appealing properties [1, 2, 3, 4, 5]. For example, graphene obtained by mechanical exfoliation of highly oriented pyrolytic graphite demonstrates ballistic electronic transport at sub-micrometer distances and outstanding carrier mobility [6]. Transport investigations revealed that electrons in graphene exhibit properties of massless Dirac fermions [7]; furthermore, anomalous quantum Hall effect [8, 9] and Josephson effect [10] were observed experimentally. However, some of the unique graphene properties may impede technological applications. As an example, the absence of a bandgap complicates the creation of graphene-based logic elements in electronics [11, 12], while optical transparency imposes limits on the responsivity of graphene-based photodetectors and solar cells [13, 14]. Covalent functionalization of graphene is a promising approach to overcome such limitations. Binding of various functional groups to the basal plane leads to disruption of the ideal $sp^2$ bound graphene structure by incorporation of $sp^3$ hybridized carbon atoms with tetrahedral bond orientation, which leads to a significant change in the transport properties of graphene. A number of studies have demonstrated the formation of a band energy gap as a result of the covalent modification [15, 16, 17].

In this study, we carry out the covalent functionalization of few-layer graphene grown on cubic-SiC/Si(001) wafers by the Neutral Red phenazine dye using the diazonium chemistry approach [18, 19, 20]. We employ this functionalization approach because of its simplicity, high degree of functionalization, and relatively short reaction time. The dye is widely utilized in a large number of biological [21, 22, 23, 24, 25] and non-biological [26, 27, 28, 29, 30] applications such as virulence markers, DNA intercalation, intracellular pH indicators, viability assay, photosensitizers, fiber-optic chemical sensors, photogalvanics and solar cells. In our experiments, the Neutral Red dye has been used for the synthesis of its diazonium salt via diazotization reaction (Fig. 1a). The aqueous solution of the salt has been placed on the graphene surface in the form of a droplet with simultaneous illumination by intense white light. It results in photoexcitation of graphene valence electrons and reduction

*E-mail: dmitrii.potorochin@xfel.eu
**E-mail: zhussupk@tcd.ie

of diazonium cations, which leads to formation of active radicals capable of covalent binding to the carbon atoms from the graphene layer accompanied by change of their hybridization from $sp^2$ to $sp^3$ (Fig. 1b).

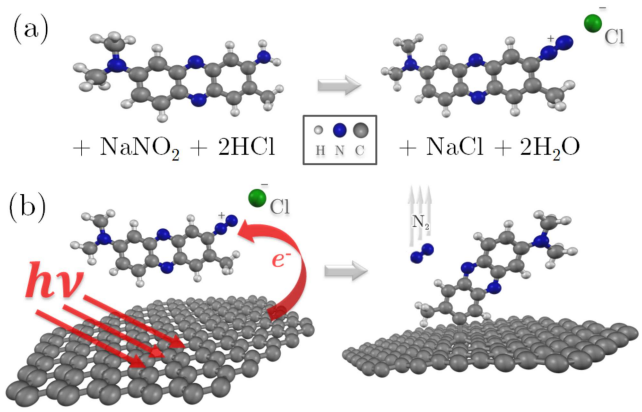


Figure 1: Principle scheme of (a) the diazotization reaction and (b) graphene functionalization.

It was previously shown by scanning tunneling microscopy (STM) [31] that the phenazine dye molecules on graphene/SiC(001) can form a locally ordered structure with molecules oriented almost perpendicular to the graphene surface and arranged in the rectangular lattice. Scanning tunneling spectroscopy (STS) revealed a bandgap opening in this phenazine dye/graphene structure [31]. In this study, we use X-ray photoelectron spectroscopy (XPS), ultraviolet photoelectron spectroscopy (UPS), ultraviolet photoemission electron microscopy (UV-PEEM), near-edge X-ray absorption fine structure (NEXAFS), and STM/STS to obtain detailed information about the atomic and electronic structure of the composite phenazine dye/graphene/SiC(001) system. XPS and UPS studies demonstrate that functionalization impacts only the top layer of the few-layer graphene, while the bottom layers remain intact and exhibit metallic properties. Detailed NEXAFS and STM studies reveal a coexistence of different locally ordered structures with phenazine derivatives both lying down and standing up on the graphene/SiC(001) surface. Density functional theory (DFT) calculations show that these structures strongly influence the overall electronic properties of the system, leading to the experimental observation of a bandgap exceeding 2 eV in some surface areas and depending on the orientations and deformations of the molecules. STS and UV-PEEM investigations suggest that the multilayer graphene-dye composite possesses functionalities that might be attractive for optoelectronic applications [32, 33, 34], taking into account the possibility of wafer-scale quasi-free standing few-layer graphene growth on $\beta$-SiC(001) and facile formation of a two-dimensional semiconducting organic layer on its surface as a result of chemical modification.

## 2. Material and methods

Few-layer graphene was epitaxially grown on $\beta$-SiC(001) using series of annealing cycles with increasing temperature up to 1550 K under ultrahigh vacuum conditions as described in the previous works [35, 36, 37, 38, 39, 40]. The lateral size of the graphene films is comparable to the dimensions of the initial silicon carbide sample [35, 36]. For the chemical modification, the graphene sample was treated ex situ by the solution of diazonium salt of the Neutral Red dye under illumination by intense white light [31, 41]. Thereafter, the specimen was washed by the flow of pure ethanol to remove all products of the reaction along with unreacted components with a further 10 minute sonication in the same solvent. Later on, the sample of dye-modified graphene was transferred to UHV where it was annealed at a temperature of about 200 °C to remove the remaining physisorbed molecules.

The XPS, UPS and NEXAFS measurements were performed at Russian-German dipole beamline of BESSY II electron storage ring operated by Helmholtz-Zentrum Berlin für Materialien und Energie [42, 43]. All preliminary studies and development of sample preparation procedures were carried out at the P04 beamline [44] of the PETRA III synchrotron radiation facility, Argus endstation [45]. This dipole-based beamline provides a moderate photon flux distributed continuously over a wide photon energy range from 30 to 1500 eV which is suitable for radiation-sensitive materials such as organic composites. Experimental station equipped with PHOIBOS 150 electron-energy analyzer (SPECS GmbH) was employed for the XPS experiments. The measurements have been conducted at room temperature in constant analyzer energy mode with a pass energy of 20 eV. The pressure in the analytical chamber was always below $5{\cdot}10^{-10}$ mbar. Deconvolution of the XPS spectra has been done using the Casa XPS software (version 2.3.16 PR 1.5). Experimental core level spectra have been fitted by synthetic lineshape composed of the sum of asymmetric Doniach-Sunjic profile [46] for graphene component, which is justified by its metallic nature and symmetric Gaussian-Lorentzian product profile for other components. Shirley-type background profile was employed to take into account the contribution of inelastically scattered electrons [47]. All XPS spectra were calibrated in reference to the Au $4f_{7/2}$ signal [48] (binding energy of 84 eV), which has been acquired after every change of beamline monochromator settings.

The NEXAFS spectra were acquired in a total electron yield (TEY) mode, i.e. drain current from the sample was measured during scanning of the photon energy of X-ray radiation. Before analysis, the spectra were normalized to the post-edge intensity where no resonances are presented: at 320 eV for C K-edge and at 415 eV for N K-edge.

The PEEM measurements were conducted using an Omicron FOCUS IS-PEEM microscope equipped with an imaging energy filter at the Russian-German Laboratory of BESSY II, Berlin. A Hg discharge lamp was used as an excitation source (4.9 eV photon energy).

The atomic structure of the SiC(001) surface during graphene synthesis was controlled in situ in a RIBER LAS-3000 spec-

trometer equipped with a room temperature (RT) scanning tunneling microscope GPI-300. The atomic and electronic structure of the graphene, ex-situ functionalized with phenazine dye Neutral Red molecules, has been studied at 77 K using low temperature STM produced by Createc. Chemically etched [001]- and [111]-oriented single-crystalline tungsten tips sharpened in UHV by electron beam heating and ion sputtering [49, 50] were used for high-resolution STM/STS experiments.

First-principles electronic structure simulations were performed using fully relativistic plane-wave self-consistent field (PWscf) DFT code from the Quantum ESPRESSO software distribution [51]. Ultrasoft pseudopotentials [52] were used and the correlation and electron exchange energies were considered within the local density approximation (LDA) with the Perdew–Zunger parametrisation [53]. The plane-wave energy cut-off is 1600 eV. The cell dimensions and atomic positions were allowed to fully relax using a per atom force threshold of $10^{-3}$ eV/A and a total energy threshold of $10^{-4}$ eV [54]. The phenazine dye molecule of 64 atoms was placed above a fixed position single graphene layer, comprised of 48 atoms, and allowed to relax towards the surface. The side and top views of the relaxed structure are presented in Figure 6(c,d). The molecule is placed in the unit cell such that the infinite repetition of the unit cell results in tightly packed rows of molecules, with a small space of 8 Å separating each row. A k-space sampling density of 12×12×1 k points was used. The out-of-plane vacuum is 15 Å in size. The XCrySDen package was used for visualising the relaxed model [55]. The density of states of the molecule is calculated using Löwdin population analysis [56].

## 3. Results and discussion

### *3.1. XPS and UPS analysis*

For fine chemical analysis of the graphene/SiC/Si(001) functionalized by the Neutral Red phenazine dye, high-resolution C 1s and N 1s spectra were decomposed onto individual components corresponding to different chemical bonds using the multipeak fitting procedure. Figure 2(b) shows the XPS N 1s spectrum of graphene/SiC(001) chemically modified by the Neutral Red dye. The appearance of the N 1s signal in the XPS spectra after the functionalization directly indicates the presence of the phenazine dye on the sample, even after sonication and annealing in ultra-high vacuum (UHV) at temperatures close to 200°C. This fact proves that chemical bonds of phenazine dye molecules with graphene overlayer are strong enough to keep them on the surface even after intense treatment. The decomposition of the spectrum shows the presence of two main components that correlate well with the chemical structure of the dye. The more pronounced peak at 398.62 eV corresponds to pyridine [57, 58], having two $\sigma$-bonds and one $\pi$-bond with carbon atoms. Its twice higher intensity is related to the presence of two nitrogen atoms of such kind in the central ring of the molecule. The second lower-intensity peak (400.56 eV) can be attributed to the single tertiary amine [59, 60] at the outer side of the molecule, bound by three $\sigma$-bonds with carbon atoms. The other two minor peaks denoted by dark blue and dark red colors are assigned to shake-up satellites. Each separated by 3.4 eV from the main peak they correspond to and exhibit a similar ratio close to 1:2. Such interpretation corroborates with the multipeak fitting analysis applied to C 1s core-level spectra, discussed below. In addition, the absence of a peak in the vicinity of 399.5 ± 0.3 eV, corresponding to primary amines [61, 62] (-$NH_2$ groups), indicates that there are no unreacted Neutral Red dye molecules on the surface. They either were ultimately converted to diazonium salt or removed from the surface during sonication and further heating in UHV. Furthermore, there is no evidence of diazonium cations that could provide features at binding energies higher than 402 eV [63, 64]. Therefore, we can conclude that all undesirable products of the reaction and pristine reactants were removed from the graphene/SiC/Si(001) surface after the functionalization and cleaning.

The result of the fitting for the C 1s XPS spectrum is presented in Figure 2(a). The dark grey component corresponds to the bulk SiC contribution which is traditionally used as a reference signal for graphene grown on cubic-SiC(001). In contrast to hexagonal SiC, it has no additional buffer layer component and reveals only one peak in the XPS spectrum at a well-known position (approx. 283 eV). The photon energy of 700 eV was intentionally utilized for the spectra acquisition to obtain a substantial reference signal from bulk SiC what allows more reliable multipeak analysis. The asymmetric red component with a binding energy of 284.43 eV corresponds to the graphene $\pi$-conjugated system. Additionally, there is a contribution of $sp^2$-hybridized carbon atoms from the dye molecules to this peak. The distance between surface graphene and bulk SiC peaks is in good agreement with our previous investigations [35, 45, 36]. The other two peaks with binding energies of 285.24 and 285.92 eV [yellow and blue components in Fig. 2(a,c)] are related to the chemically modified graphene. The yellow component corresponds to the signal from $sp^3$ hybridized carbon atoms [61, 65]. This component initially originates from the dye molecule, but also emerges in the graphene layer after attachment of the Neutral Red to the graphene basal plane, since the formation of a new sigma bond requires a change of hybridization of the carbon atoms from $sp^2$ to $sp^3$. This disruption of the ideal $sp^2$-bound graphene structure leads to the bandgap opening, as has been shown in the previous studies [15, 16, 17, 31]. The blue curve corresponds to the signal from $sp^2$ hybridized carbon atoms covalently bound to nitrogen [61, 62]. The features denoted by dark red and dark blue colors and observed at higher binding energies can be explained by several shake-up satellites that arise due to the electron energy loss related to the excitation of the valence band electrons of the chemically modified graphene. The energy shifts of the satellites from the main peaks in C 1s and N 1s spectra are also equal to 3.4 eV, which adds weight to this assumption. Finally, the green peak around 291 eV binding energy can be assigned to shake-up satellite typical of graphene. It emerges as a result of energy loss of electrons from the main graphene peak for graphene valence electrons transitioning to $\pi^*$-states [65, 66]. This can serve as an additional sign of pristine metallic graphene presence in the composite system.

Apart from the shake-up satellite, a strong signal from $sp^2$

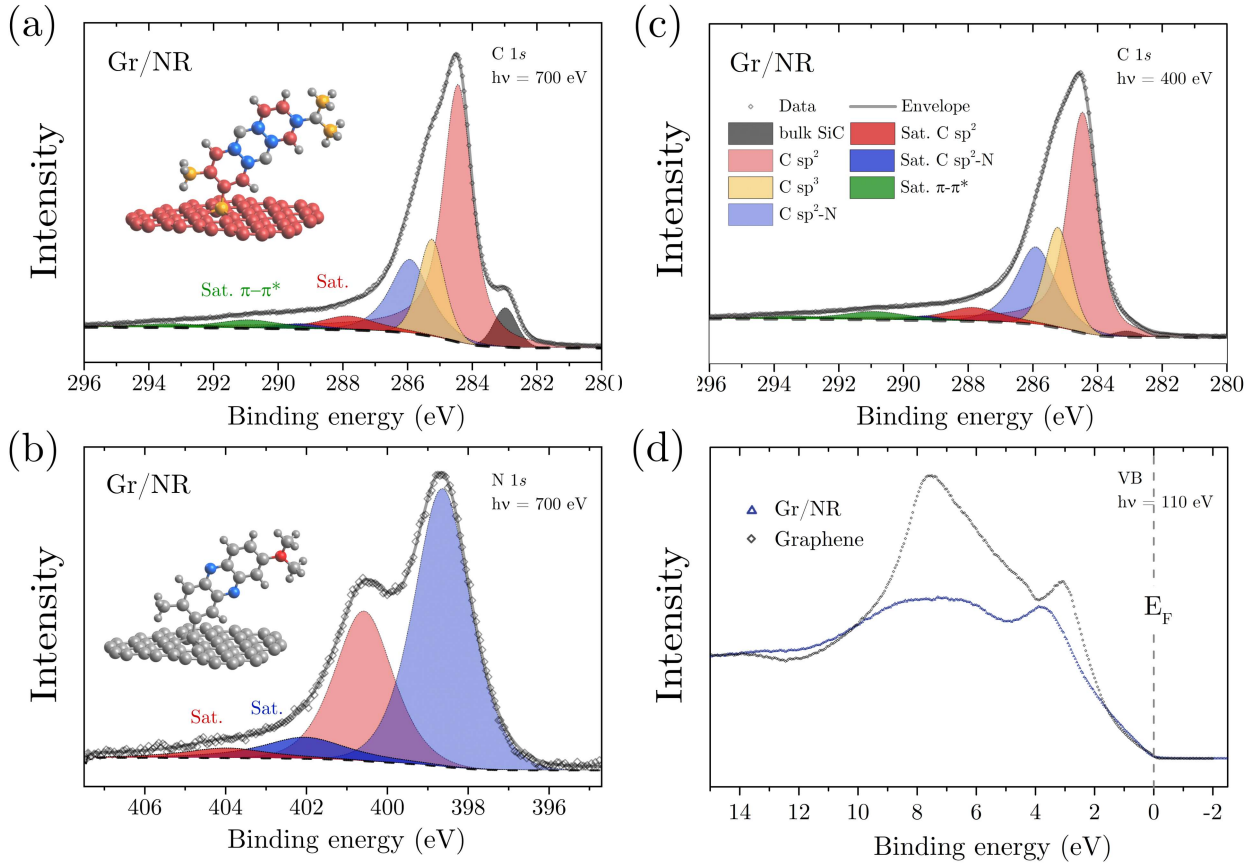


Figure 2: High-resolution (a) C 1s and (b) N 1s core-level photoemission spectra of few-layer graphene sample epitaxially grown on cubic-SiC/Si(001) chemically modified by Neutral Red dye derivatives recorded using 700 eV photon energy. (c) High-resolution C 1s spectrum of the same sample recorded using 400 eV photon energy for surface sensitivity increase. (d) High-resolution UPS valence band spectra of the sample before (Graphene) and after (Gr/NR) functionalization recorded using 110 eV photon energy.

electron states demonstrates that the $sp^2$-bound structure of the top graphene layer is only partially disrupted by the functionalization. Besides, we can suggest that subsurface graphene layers are not substantially modified. This suggestion is supported by a comparison of C 1s XPS spectra acquired at different photon energies [Fig. 2(a,c)]. An increase in the kinetic energy of the electrons extracted from the core-level by 300 eV (an increase in the photon energy from 400 eV to 700 eV) leads to a substantial increase in the bulk sensitivity of the XPS spectra, caused by an increase of the inelastic mean free path of photoelectrons by a factor of two [67]. Enhancement of the signal associated with graphene and SiC substrate in conjunction with suppression of the component associated with dye-modified graphene prove that the bottom layers of the few-layer graphene grown on $\beta$-SiC(001) indeed remain intact. On the other hand, we can observe an increase in the intensity of the dye-specific peaks (blue and yellow curves) relative to the graphene peak (red curve) by 32 % in surface-sensitive mode (400 eV photon energy). This proves a layered structure of the phenazine dye/graphene structure where Neutral Red dye derivatives are aggregated on the surface while non-modified graphene lies beneath them.

Another sign of the presence of non-modified graphene layers in the system can be obtained via comparison of graphene UPS spectra before and after functionalization recorded at 110 eV photon energy, representing occupied valence states [Fig. 2(d)]. One can see that valence states of the SiC substrate in the region of 5-9 eV are no longer visible after the functionalization because the inelastic mean free path of photoelectrons becomes insufficient for observing the substrate signal after adding an extra layer consisting of dye molecules on top of the few-layer graphene on cubic-SiC(001) sample. However, one can observe a prominent signal in the energy region close to the Fermi level both before and after chemical modification. Therefore, we can conclude that underlying non-modified graphene layers continue to exhibit metallic properties. Otherwise, a bandgap would be observed.

### 3.2. *NEXAFS studies*

For a better understanding of the atomic and electronic structure of the graphene-dye nanocomposite, we investigated its unoccupied electronic states with NEXAFS technique. Moreover, linear polarization of the light gives us a possibility to determine the preferential orientation of the phenazine deriva-

tives on the millimeter-size graphene/SiC(001) samples using the absorption anisotropy. Change of the relative intensity of the peaks, corresponding to excitations from core levels to $\pi^*$ or $\sigma^*$ molecular orbitals during the sample rotation relative to the electric field vector of the probing light, provides valuable information about the spatial orientation of molecules. According to the dipole selection rules, the probability of photon absorption depends on the angle between the electric field vector and the orientation of the molecular orbital. [68, 69] In terms of our study, that means that maximal $\pi^*$ resonance can be observed for planar $\pi$ conjugated system when the electric field vector is oriented perpendicular to the molecular plane while maximal $\sigma^*$ signal should be observed when the electric field vector is oriented parallel to it.

Figure 3(a) shows the C K-edge NEXAFS spectra of graphene functionalized by the Neutral Red dye measured at four different photon beam incidence angles. One can see three $\pi^*$-resonances in the photon energy range of 285-291 eV [70, 71, 72]. The first resonance ($\sim$ 285.9 eV) corresponds to carbon-carbon bonds and predominantly originates from the graphene $sp^2$ bound system. However, two benzene-type rings of the dye also contribute to this signal which must be taken into account during analysis of the absorption anisotropy. The next resonance ($\sim$ 287 eV) corresponds to the carbon-nitrogen bonds in the molecules. This peak in the NEXAFS spectra can be utilized as a marker for determination of molecular orientation. The third peak in the 285-291 eV photon energy range can be attributed to the carbon-nitrogen $2\pi^*$-resonance. In the region of photon energies above 291 eV, $\sigma^*$-resonances are observed. The intermixing of $\sigma^*$-resonances from all layers of the complex nanocomposite (silicon carbide, graphene, and organic molecules) leads to the resulting plateau-like bump, which can serve as a reference signal for the $\pi^*$-resonances measured at different photon incidence angles.

In the normal incidence geometry (indicated as 0° in Fig. 3), the electric field vector is parallel to the surface. In this case, the signal from the $\pi^*$-resonance of graphene should be negligible [35]. Previous local STM studies of graphene grown on $\beta$-SiC(001) modified by the Neutral Red dye through a diazonium chemistry approach revealed that dye molecules may form a composite structure with short-range order. The molecules in this structure are oriented almost perpendicular to the graphene surface and arranged in a rectangular lattice [31]. The NEXAFS spectrum measured in the normal incidence geometry shows a strong carbon-nitrogen $\pi^*$-resonance that can be attributed to standing up dye molecules. However, changing the photon beam incidence angle closer to grazing incidence does not lead to diminishing this resonance. Moreover, the $\pi^*$-resonance slightly grows with increasing incidence angle. This can be explained by the presence of planar dye aggregates on the graphene surface, along with standing up dye molecules. These aggregates must be strongly bound to the graphene surface; otherwise, they would not stand the stiff treatment that was employed during the sample preparation.

To confirm the trends of the C K-edge NEXAFS spectra, nitrogen K-edge X-ray absorption has been studied. The absorption anisotropy of the N K-edge NEXAFS spectra recorded

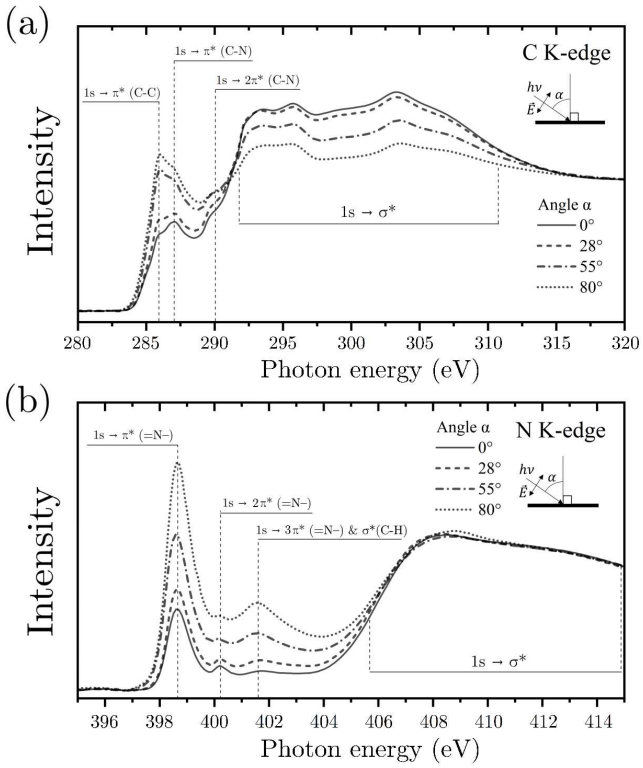


Figure 3: The (a) carbon and (b) nitrogen NEXAFS spectra of dye-modified graphene recorded along with variation relative to the sample surface plane of the electric field vector incidence angle of linearly polarized X-ray radiation. The angle $\alpha$ determines the orientation of the X-ray beam relative to the normal of the sample. The angle of 0° corresponds to the case when the electric field vector is parallel to the sample surface; the angle of 90° means that the electric field vector is perpendicular to it.

at the same four X-ray incidence angles is presented in Figure 3(b). One can distinguish three $\pi^*$-resonances in the photon energy range of 398-405 eV, which closely resemble the experimental and theoretical NEXAFS spectra of pyridine [73, 74, 75]. The resonances at 398.6 eV, 400.2 eV, and 401.6 eV can be assigned to transitions to $1\pi^*$, $2\pi^*$, and energetically close $3\pi^*$ and $\sigma^*$(C-H) orbitals, respectively. The resonances are related to the middle phenazine ring containing two $sp^2$-hybridized nitrogen atoms, serving as a conjunction between two benzol rings. The absorption spectra, shown in Figure 3(b), demonstrate that the change of X-ray incidence angle from normal to grazing incidence leads to substantial growth of $\pi^*$-resonances. Therefore, we can conclude that the $\pi$-orbitals of the dye derivatives predominantly tend to align with the sample normal, i.e., the molecular plane is more likely to be parallel to the surface, which is in contrast with the model of standing up molecules [31]. Nevertheless, even at the normal incidence of X-rays, the first $\pi^*$-resonance at 398.6 eV remains noticeable, which does not exclude the presence of standing up molecules on the graphene surface. Summarizing the absorption anisotropy experiments, both N and C K-edge NEXAFS spectra suggest a complex morphology of the Neutral Red/graphene composite structure with molecules both stand-

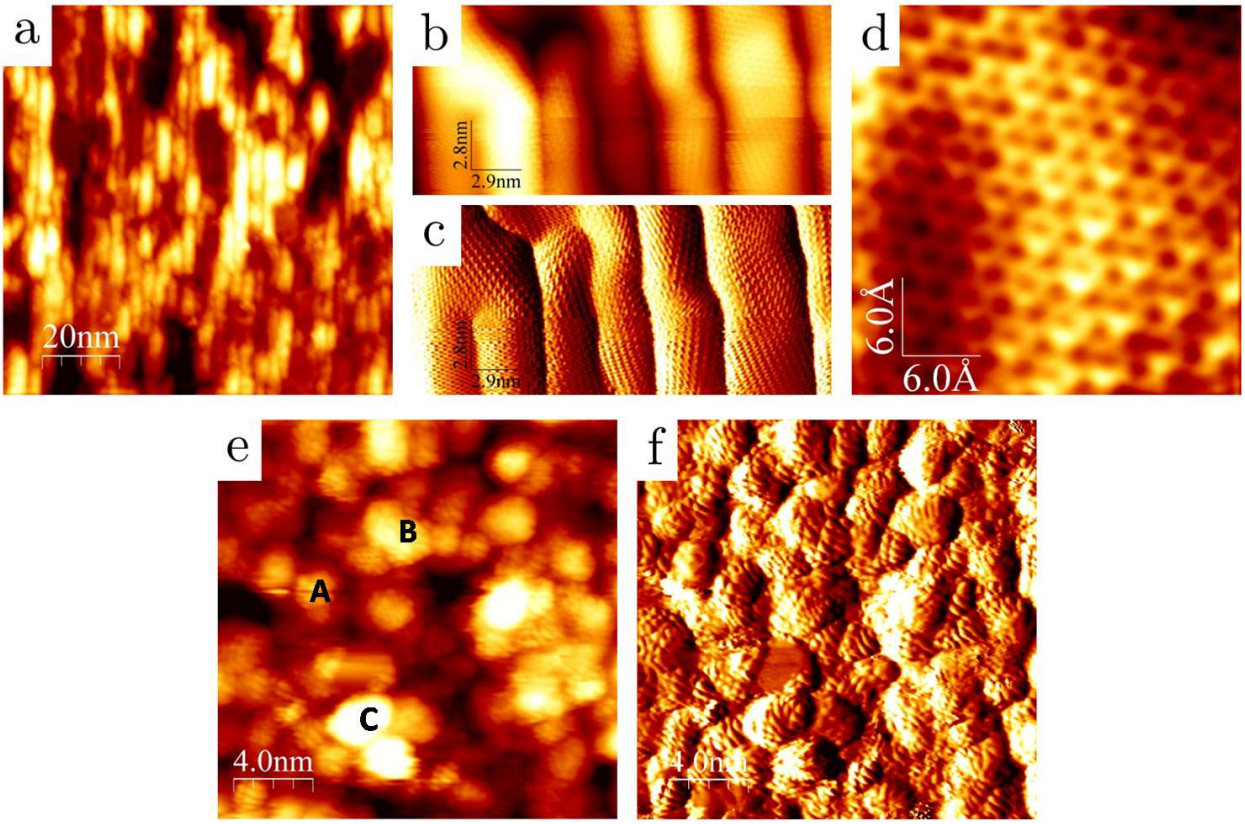


Figure 4: STM images of graphene/SiC(001) before (a-d) and after (e,f) functionalization by Neutral Red dye molecules. The images (c) and (f) were obtained after dZ/dX differentiations of the topography images shown in panels (b) and (e), respectively.

ing up and lying down on the graphene surface.

### *3.3. STM/STS studies*

Detailed STM studies conducted in different surface areas of the functionalized graphene/SiC(001) sample showed that the dye molecules can form different structures with molecules oriented both parallel and perpendicular to the surface. Prior to functionalization, STM studies of the graphene/SiC(001) sample revealed typical nanodomain structure with rotated graphene lattices [37, 38, 39, 40] and boundaries preferentially oriented along the <110> directions of the SiC crystal lattice [Fig. 4(a-c)]. Inside the domains, high-resolution STM images revealed randomly distorted honeycomb lattice typical of few-layer graphene grown on the cubic-SiC/Si(001) substrates [Fig. 4(d)].

STM images of graphene after the chemical modification [Fig. 4(e) and 4(f)] show a more complicated structure with increased roughness [Fig. 4(e)]. According to high-resolution STM data, the composite structures with both standing and lying molecules can be found on the functionalized graphene/SiC(001) sample. Figures 4(e) and 4(f) show the surface area where most of the molecules are lying down. From the STM data we can suggest that lying molecules preferentially form dimer structures, as schematically shown in Figures 5(e) and 5(f). The phenazine dye molecules in these structures are not ideally parallel to the graphene surface in agreement with slightly increased surface roughness after functionalization [Fig. 4(e)].

Figure 5(e) shows the surface area with coexisting standing molecules (top left corner) and lying dimers (bottom part of the image). A higher resolution image of the surface area with standing up molecules is shown in Figure 5(b). Note that standing molecules in this case form an oblique cell with unit vectors of approximately 3.5 and 4.5 Å [Fig. 5(c,d)] rather than rectangular cell reported in earlier studies [31]. Both these structures with different short-range order for standing molecules can be observed on the functionalized graphene/SiC(001) sample in different surface areas.

STS experiments conducted in various surface regions showed a substantial difference in the electronic structure of the composites with standing and lying molecules. As revealed our previous STS and DFT studies, the phenazine dye/graphene structure with standing up molecules demonstrates an energy gap of about 0.8 eV [31]. STS experiments performed in the surface areas with phenazine derivatives oriented preferentially parallel to the surface revealed an increase in the energy gap, which could exceed 2.0 eV. Figure 6(a) shows three dI/dV spectra measured in different surface areas containing the phenazine dye dimers oriented parallel to the surface. The experimental STS spectra demonstrate that energy gap varies along the surface and exceeds 0.8 eV substantially in all surface areas with the phenazine dye derivatives, which are preferentially ly-

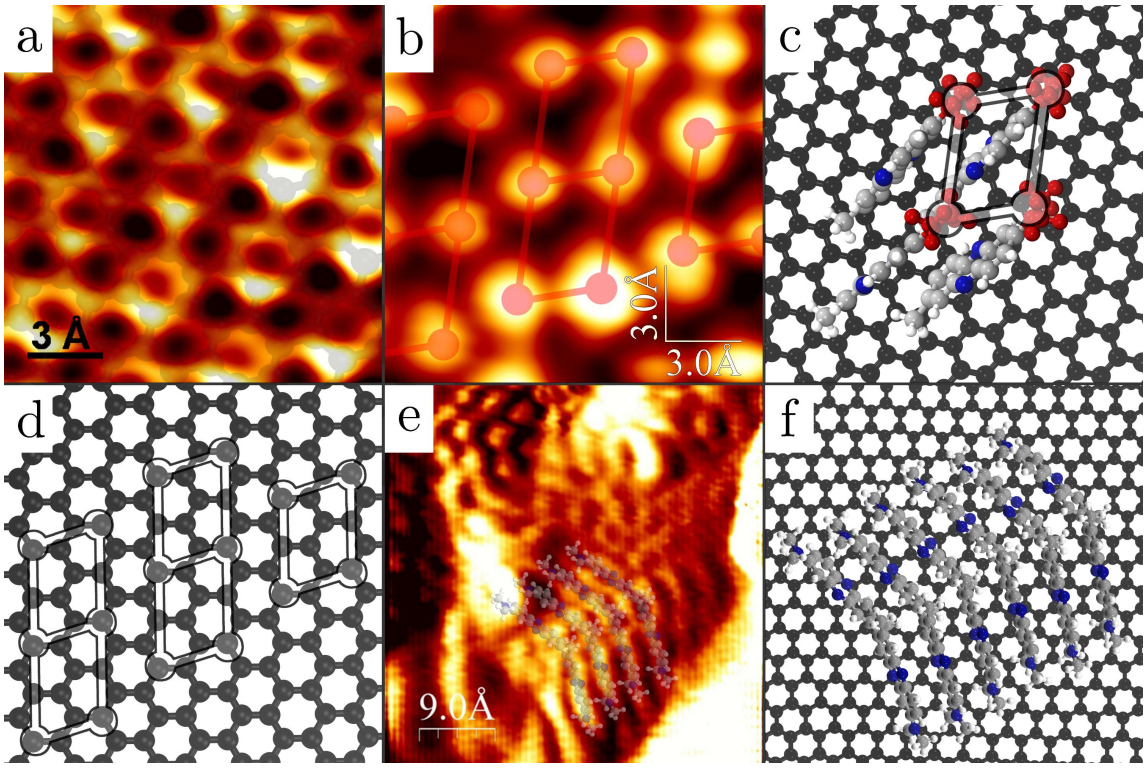


Figure 5: 1.5x1.5 nm$^2$ STM images of graphene/SiC(001) before (a) and after (b) functionalization. The image in panel (b) shows the surface areas with short-range order where molecules are oriented perpendicular to the surface. Such kind of nanostructure is formed according to the pathway represented in Figure 1(b). A schematic representation of standing molecules having the short-range order is presented in (c). Two methyl groups on the side of the phenazine dye derivative are highlighted by red in (c) because presumably, the current of electrons from their occupied states leads to the observation of the bright protrusions in (b). Panel (d) shows an overlay of the oblique unit cells from (b) on the graphene lattice. A mismatch of the molecular and graphene cells leads to an in-plane shift of the molecular cells. Panel (f) shows a schematic representation of lying Neutral Red dimers observed in (e).

ing down. Although the fine structure of the tunneling spectra varies from one surface area to another, the position of the valence band maximum is approximately the same in all experimental spectra [Fig. 6(a)]. At the same time, the position of the conduction band minimum shifts by several hundred meV, indicating local modifications of the electronic structure of the phenazine dye/graphene composite.

### *3.4. DFT calculations*

For explanation of the experimental STS and photoemission data and understanding the structural and electronic properties of the phenazine dye derivatives on graphene/SiC/Si(001) wafers, fully-relaxed DFT calculations were employed. The calculated density of electron states (DOS) for the molecules lying on the graphene surface is shown in Figure 6(b) (black curve). The model of the phenazine dye/graphene structure used in the calculations is presented in Figure 6(c,d) (side and top views). The DFT calculations show that the fully relaxed molecule on the graphene surface has a bandgap of approximately 0.74 eV, diverging from the experimental STS and UPS data demonstrating substantially larger energy gap for the composite structures with molecules lying down on the graphene surface [e.g., see STS spectra in Fig. 4(a)]. This DFT calculation considered the molecule in the unit cell to be attached to an ideal flat graphene surface, without taking into account the complexity of the molecules' environment. According to the STM data [Fig. 5(e,f)], one may anticipate both local deformations of the molecules because of the roughness of the pristine nanostructured graphene and conjunction molecules to one another.

In order to simulate the phenazine dye derivatives in a higher density environment, further calculations were conducted. The relaxed molecule was compressed in both the in-plane directions by 5%, 10%, and 15%, and the resulting electronic structure of these calculations was investigated. The DOS of the compressed molecules are presented in Figure 6(b) alongside that of the fully relaxed molecule. The fundamental bandgap is calculated to be 0.95 eV for 5%, 1.17 eV for 10% and 1.36 eV for 15%, respectively. It should be noted that the bandgap of the phenazine dye dimer is increasing with increasing compression of the molecule [76]. The calculated DOS of the compressed molecules demonstrate almost unchanged position of the valence band maximum and gradual shift of the conduction band minimum, which is in qualitative agreement with the results of the STS experiments [Fig. 6(a)]. This observation suggests that compressed molecules behave like a p-type semiconductor [77].

This theoretical compressive study on the molecule demonstrates how mechanical compression can modify the electronic properties of the phenazine derivatives. The results of the cal-

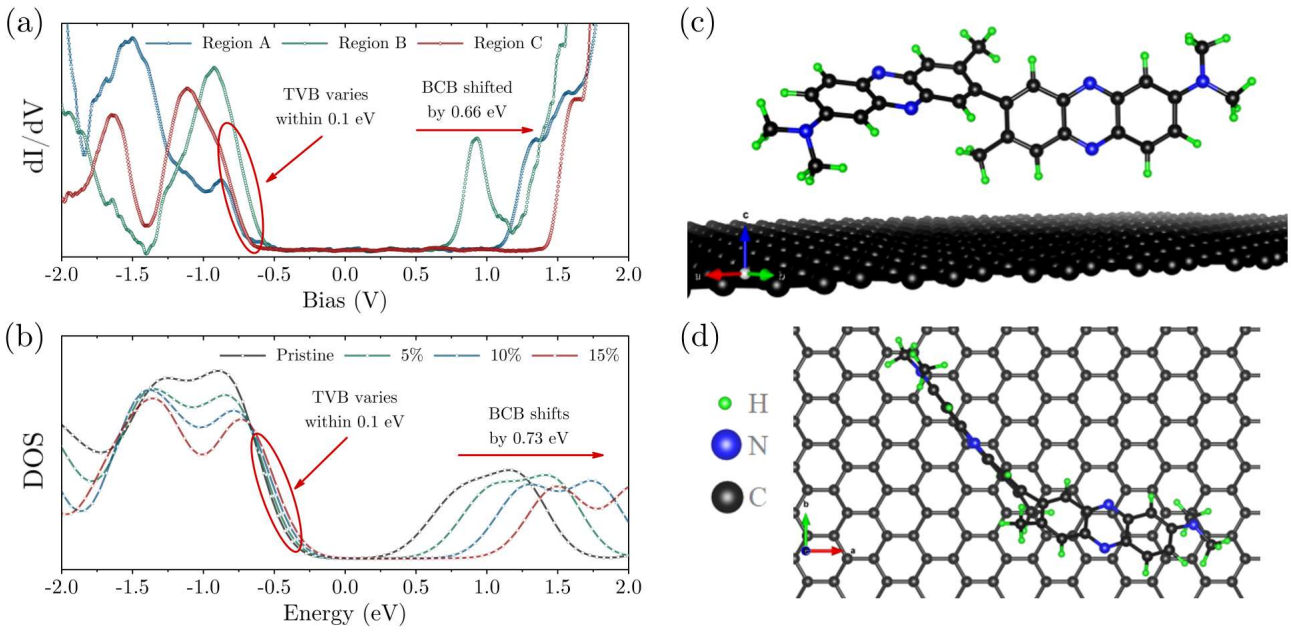


Figure 6: (a) STS spectra measured in different surface areas above phenazine dye derivatives oriented parallel to the surface (indicated A, B, and C in Fig. 4(e)). (b) Calculated DOS of the lying molecule as function of the molecule compression along x and y directions. (c) and (d) relaxed structure of the phenazine dye dimer on top of the graphene with side and top views, respectively.

culations can explain the obtained experimental variation of the bandgap in the composite phenazine dye/graphene structure with molecules parallel to the surface.

### *3.5. PEEM imaging*

Figures 7(a,b) present UV-PEEM images of graphene grown on $\beta$-SiC(001) before and after chemical modification by the Neutral Red dye derivatives. Slight intensity variations on micrometer scale for pristine graphene sample [Fig. 7(a)] are justified by the presence of two types of antiphase domains (APDs) on SiC(001) substrate [36]. The domains are typical of $\beta$-SiC(001) grown by chemical vapor deposition on silicon wafers [37, 38]. The crystal structure of the domains is rotated by 90° relative to one another. The APD boundaries can exhibit a slight variation of the work function, which can be observed in UV-PEEM images. Investigation of the dye-modified sample [Fig. 7(b)] shows homogeneity even on a larger scale, despite heterogeneity observed by STM and STS measurements expressed in observation of two types of nanostructures on the surface with variable bandgap. However, the heterogeneity encountered on the nanometer scale is averaged on the micrometer scale, which leads to the overall homogeneity of the electronic properties. Another important observation from the UV-PEEM data is the absence of non-modified graphene regions. According to XPS measurements, one can observe silicon carbide substrate signal in C 1s core-level spectrum recorded at 700 eV photon energy [Fig. 2(a)]. Taking into account the inelastic mean free path of photoelectrons in this case ($\sim$ 2 nm), we can conclude that the introduced dye-containing layer is thinner than 2 nm. Even though, there are no surface regions not covered by the phenazine derivatives after the multistep sample cleaning procedure. Figure 7(c) displays a comparison of secondary electron spectra taken from graphene before and after the chemical modification. The kinetic energy position of the onset of the secondary electron signal allows determining the sample work function. One can see that chemical modification of graphene on $\beta$-SiC(001) leads to a noticeable work function increase from approximately 4 eV to 4.3 eV, indicating electronic properties modification as a result of functionalization.

## 4. Conclusions

A method of functionalization of graphene synthesized on $\beta$-SiC/Si(001) wafers based on the chemistry of diazonium compounds has been discussed. The advantages of this method are its simplicity, the high degree of functionalization, and the relatively short reaction time. Neutral Red dye/graphene composite has shown high stability verified by XPS measurements after sonication and annealing in ultra-high vacuum conditions. STM and NEXAFS studies have demonstrated that dye molecules can form different locally ordered structures with molecules oriented almost parallel or perpendicular to the surface. In the latter case the molecules are standing up on the graphene surface and exhibit a short-range order with either rectangular or oblique unit cell. In the former case, the dye molecules form planar dimer structures bound with the graphene/SiC(001) sample. UV-PEEM imaging proves the homogeneity of the system on a large scale. STS measurements and secondary electron cutoff revealed a modification of the electronic structure during the functionalization, which results in the emergence of a bandgap in the density of states of the phenazine dye/graphene system in some cases exceeding 2 eV

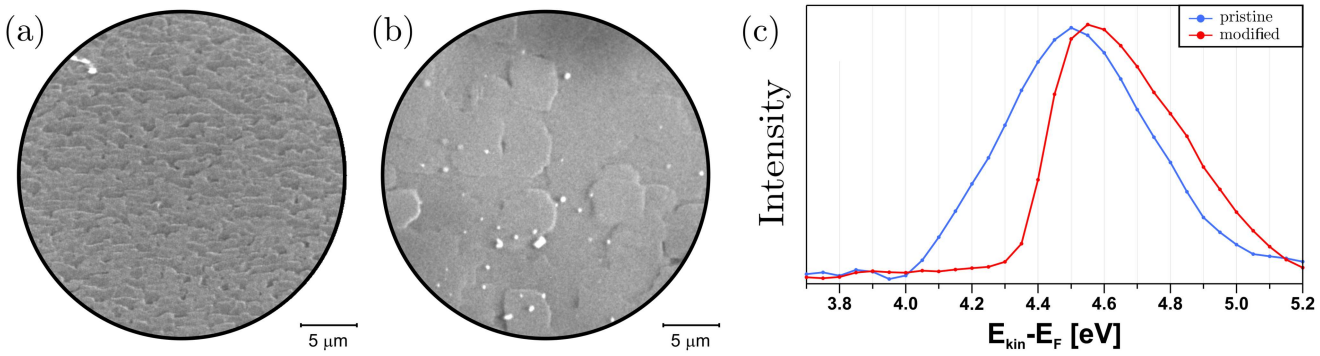


Figure 7: UV-PEEM images of graphene grown on $\beta$-SiC(001) before (a) and after chemical modification by the Neutral Red organic dye using the diazonium chemistry approach. (c) Secondary electron cutoff, which represents the work function change as a result of the chemical modification of graphene/SiC(001).

and a change of the work function. According to the DFT calculations, the local variations of the bandgap in the functionalized graphene may be related to deformations of the molecules in the composite structure. Besides, XPS and UPS analysis shows that the bottom layers of the few-layer graphene remain intact, which inherently makes the synthesized layered composite a low-dimensional metal/semiconductor heterostructure.

## Author Contributions

D.V. Potorochin: Formal analysis, Investigation, Visualization, Writing – original draft. A.N. Chaika: Formal analysis, Investigation, Visualization, Writing – original draft. O.V. Molodtsova: Conceptualization, Investigation, Writing – review & editing. V.Yu. Aristov: Conceptualization, Investigation, Writing – review & editing. D.E. Marchenko: Investigation, Visualization, Formal analysis. D.A. Smirnov: Investigation, Formal analysis. A.A. Makarova: Investigation, Formal analysis. B. Walls: Investigation, Visualization, Writing – review & editing. K. Zhussupbekov: Formal analysis, Investigation, Visualization, Writing – original draft. K. Walshe: Formal analysis, Investigation, Visualization, Writing – original draft. I.V. Shvets: Investigation, Resources, Conceptualization. A.S. Ciobanu: Investigation, Resources. M.K. Rabchinskii: Methodology, Validation. N.V. Ulin: Methodology, Validation. M.V. Baidakova: Methodology, Validation. P.N. Brunkov: Conceptualization, Project administration, Resources. S.L. Molodtsov: Conceptualization, Project administration, Resources.

## Conflicts of interest

The authors declare that they have no known competing financial interests or personal relationships that could have appeared to influence the work reported in this paper.

## Acknowledgements

This work was carried out within the framework of the state assignment of the ISSP RAS and partially supported by the Russian Foundation for Basic Research (Grant no. 20-02-00489) and Erasmus plus mobility grant (2016-1-IE02-KA107-000479). I.V.S. and K.Z. acknowledge the support of the IRC LA (IRCLA/2019/171). A.A.M. and D.A.S. acknowledge the BMBF (grant no. 05K19KER and 0519ODR, respectively). M.K.R. and M.V.B. work on the functionalization of few-layer graphene by Neutral red organic dye was supported by the Ministry of Science and Higher Education of the Russian Federation (agreement no. 15.CUH.21.0003). K.Z. would like to acknowledge the support of the Kazakh government under the Bolashak program. Authors thank the Helmholtz-Zentrum Berlin für Materialien und Energie for the allocation of synchrotron radiation beamtime and support within the bilateral Russian-German Laboratory program.

## References

[1] A. H. Castro Neto, F. Guinea, N. M. R. Peres, K. S. Novoselov, A. K. Geim, The electronic properties of graphene, Rev. Mod. Phys. 81 (2009) 109–162. doi:10.1103/RevModPhys.81.109.
URL https://link.aps.org/doi/10.1103/RevModPhys.81.109

[2] I. Frank, D. M. Tanenbaum, A. M. van der Zande, P. L. McEuen, Mechanical properties of suspended graphene sheets, Journal of Vacuum Science & Technology B: Microelectronics and Nanometer Structures Processing, Measurement, and Phenomena 25 (6) (2007) 2558–2561.

[3] E. Pop, V. Varshney, A. K. Roy, Thermal properties of graphene: Fundamentals and applications, MRS bulletin 37 (12) (2012) 1273–1281.

[4] L. Falkovsky, Optical properties of graphene, Journal of Physics: Conference Series 129 (1) (2008) 012004.

[5] Y. Zhu, S. Murali, W. Cai, X. Li, J. W. Suk, J. R. Potts, R. S. Ruoff, Graphene and graphene oxide: synthesis, properties, and applications, Advanced materials 22 (35) (2010) 3906–3924.

[6] K. S. Novoselov, A. K. Geim, S. V. Morozov, D. Jiang, Y. Zhang, S. V. Dubonos, I. V. Grigorieva, A. A. Firsov, Electric field effect in atomically thin carbon films, Science 306 (5696) (2004) 666–669.

[7] K. S. Novoselov, A. K. Geim, S. V. Morozov, D. Jiang, M. I. Katsnelson, I. V. Grigorieva, S. V. Dubonos, A. A. Firsov, Two-dimensional gas of massless dirac fermions in graphene, Nature 438 (7065) (2005) 197–200. doi:10.1038/nature04233.
URL https://doi.org/10.1038/nature04233

[8] Y. Zhang, Y.-W. Tan, H. L. Stormer, P. Kim, Experimental observation of the quantum hall effect and berry's phase in graphene, Nature 438 (7065) (2005) 201.

[9] Y. Zhang, Z. Jiang, J. Small, M. Purewal, Y.-W. Tan, M. Fazlollahi, J. Chudow, J. Jaszczak, H. Stormer, P. Kim, Landau-level splitting in graphene in high magnetic fields, Physical review letters 96 (13) (2006) 136806.

[10] H. B. Heersche, P. Jarillo-Herrero, J. B. Oostinga, L. M. Vandersypen, A. F. Morpurgo, Bipolar supercurrent in graphene, Nature 446 (7131) (2007) 56.

[11] S. Y. Zhou, G.-H. Gweon, A. Fedorov, d. First, PN, W. De Heer, D.-H. Lee, F. Guinea, A. C. Neto, A. Lanzara, Substrate-induced bandgap opening in epitaxial graphene, Nature materials 6 (10) (2007) 770.

[12] F. Xia, D. B. Farmer, Y.-m. Lin, P. Avouris, Graphene field-effect transistors with high on/off current ratio and large transport band gap at room temperature, Nano letters 10 (2) (2010) 715–718.

[13] K. S. Novoselov, V. I. Falko, L. Colombo, P. Gellert, M. Schwab, K. Kim, A roadmap for graphene, Nature 490 (7419) (2012) 192.

[14] F. Bonaccorso, Z. Sun, T. Hasan, A. Ferrari, Graphene photonics and optoelectronics, Nature photonics 4 (9) (2010) 611.

[15] J. Choi, K.-J. Kim, B. Kim, H. Lee, S. Kim, Covalent functionalization of epitaxial graphene by azidotrimethylsilane, The Journal of Physical Chemistry C 113 (22) (2009) 9433–9435. doi:10.1021/jp9010444.
URL https://doi.org/10.1021/jp9010444

[16] S. Niyogi, E. Bekyarova, M. E. Itkis, H. Zhang, K. Shepperd, J. Hicks, M. Sprinkle, C. Berger, C. N. Lau, W. A. deHeer, E. H. Conrad, R. C. Haddon, Spectroscopy of covalently functionalized graphene, Nano Letters 10 (10) (2010) 4061–4066. doi:10.1021/nl1021128.
URL https://doi.org/10.1021/nl1021128

[17] V. Georgakilas, M. Otyepka, A. B. Bourlinos, V. Chandra, N. Kim, K. C. Kemp, P. Hobza, R. Zboril, K. S. Kim, Functionalization of graphene: Covalent and non-covalent approaches, derivatives and applications, Chemical Reviews 112 (11) (2012) 6156–6214. doi:10.1021/cr3000412.
URL https://doi.org/10.1021/cr3000412

[18] J. Greenwood, T. H. Phan, Y. Fujita, Z. Li, O. Ivasenko, W. Vanderlinden, H. Van Gorp, W. Frederickx, G. Lu, K. Tahara, Y. Tobe, H. Uji-i, S. F. L. Mertens, S. De Feyter, Covalent modification of graphene and graphite using diazonium chemistry: Tunable grafting and nanomanipulation, ACS Nano 9 (5) (2015) 5520–5535. doi:10.1021/acsnano.5b01580.

[19] J. Park, M. Yan, Covalent functionalization of graphene with reactive intermediates, Accounts of chemical research 46 (1) (2012) 181–189.

[20] D. P. Martin, A. Tariq, B. D. O. Richards, G. Jose, S. A. Krasnikov, A. Kulak, N. N. Sergeeva, White light induced covalent modification of graphene using a phenazine dye, Chemical Communications 53 (2017) 10715–10718. doi:10.1039/C7CC05158A.
URL http://dx.doi.org/10.1039/C7CC05158A

[21] P.-J. Cardona, C. Soto, C. Martin, B. Giquel, G. Agusti, E. Guirado, T. Sirakova, P. Kolattukudy, E. Julian, M. Luquin, Neutral-red reaction is related to virulence and cell wall methyl-branched lipids in mycobacterium tuberculosis, Microbes and infection 8 (1) (2006) 183–190.

[22] Y. T. Wang, F. L. Zhao, K. A. Li, S. Y. Tong, Molecular spectroscopic study of dna binding with neutral red and application to assay of nucleic acids, Analytica chimica acta 396 (1) (1999) 75–81.

[23] J. C. LaManna, K. A. McCracken, The use of neutral red as an intracellular ph indicator in rat brain cortex in vivo, Analytical biochemistry 142 (1) (1984) 117–125.

[24] R. Fautz, B. Husein, C. Hechenberger, Application of the neutral red assay (nr assay) to monolayer cultures of primary hepatocytes: rapid colorimetric viability determination for the unscheduled dna synthesis test (uds), Mutation Research/Environmental Mutagenesis and Related Subjects 253 (2) (1991) 173–179.

[25] B. B. Fischer, A. Krieger-Liszkay, R. I. Eggen, Photosensitizers neutral red (type i) and rose bengal (type ii) cause light-dependent toxicity in chlamydomonas reinhardtii and induce the gpxh gene via increased singlet oxygen formation, Environmental science & technology 38 (23) (2004) 6307–6313.

[26] J. Goicoechea, C. R. Zamarreño, I. Matias, F. Arregui, Optical fiber ph sensors based on layer-by-layer electrostatic self-assembled neutral red, Sensors and Actuators B: Chemical 132 (1) (2008) 305–311.

[27] D. Jeon, W. J. Yoo, J. K. Seo, S. H. Shin, K.-T. Han, S. G. Kim, J.-Y. Park, B. Lee, Fiber-optic ph sensor based on sol-gel film immobilized with neutral red, Optical review 20 (2) (2013) 209–213.

[28] J. Bauldreay, M. Archer, Dye-modified electrodes for photogalvanic cells, Electrochimica Acta 28 (11) (1983) 1515–1522.

[29] A. K. Jana, B. B. Bhowmik, Enhancement in power output of solar cells consisting of mixed dyes, Journal of Photochemistry and Photobiology A: Chemistry 122 (1) (1999) 53–56.

[30] A. K. Jana, Solar cells based on dyes, Journal of Photochemistry and Photobiology A: Chemistry 132 (1-2) (2000) 1–17.

[31] N. N. Sergeeva, A. N. Chaika, B. Walls, B. E. Murphy, K. Walshe, D. P. Martin, B. D. O. Richards, G. Jose, K. Fleischer, V. Y. Aristov, O. V. Molodtsova, I. V. Shvets, S. A. Krasnikov, A photochemical approach for a fast and self-limited covalent modification of surface supported graphene with photoactive dyes, Nanotechnology 29 (27) (2018) 275705. doi:10.1088/1361-6528/aabf11.

[32] A. Stergiou, R. Cantón-Vitoria, M. N. Psarrou, S. P. Economopoulos, N. Tagmatarchis, Functionalized graphene and targeted applications – highlighting the road from chemistry to applications, Progress in Materials Science 114 (2020) 100683. doi:10.1016/j.pmatsci.2020.100683.
URL https://doi.org/10.1016/j.pmatsci.2020.100683

[33] M.-E. Ragoussi, G. Katsukis, A. Roth, J. Malig, G. de la Torre, D. M. Guldi, T. Torres, Electron-donating behavior of few-layer graphene in covalent ensembles with electron-accepting phthalocyanines, Journal of the American Chemical Society 136 (12) (2014) 4593–4598. doi:10.1021/ja411830x.
URL https://doi.org/10.1021/ja411830x

[34] G. Bottari, M. Á. Herranz, L. Wibmer, M. Volland, L. Rodríguez-Pérez, D. M. Guldi, A. Hirsch, N. Martín, F. D'Souza, T. Torres, Chemical functionalization and characterization of graphene-based materials, Chemical Society Reviews 46 (15) (2017) 4464–4500. doi:10.1039/c7cs00229g.
URL https://doi.org/10.1039/c7cs00229g

[35] V. Y. Aristov, G. Urbanik, K. Kummer, D. V. Vyalikh, O. V. Molodtsova, A. B. Preobrajenski, A. A. Zakharov, C. Hess, T. Hänke, B. Büchner, I. Vobornik, J. Fujii, G. Panaccione, Y. A. Ossipyan, M. Knupfer, Graphene synthesis on cubic sic/si wafers. perspectives for mass production of graphene-based electronic devices, Nano Letters 10 (3) (2010) 992–995. doi:10.1021/nl904115h.

[36] V. Y. Aristov, A. N. Chaika, O. V. Molodtsova, S. V. Babenkov, A. Locatelli, T. O. Menteş, A. Sala, D. Potorochin, D. Marchenko, B. Murphy, B. Walls, K. Zhussupbekov, I. V. Shvets, Layer-by-layer graphene growth on $\beta$-SiC/si(001), ACS Nano 13 (1) (2019) 526–535. doi:10.1021/acsnano.8b07237.
URL https://doi.org/10.1021/acsnano.8b07237

[37] A. N. Chaika, O. V. Molodtsova, A. A. Zakharov, D. Marchenko, J. Sánchez-Barriga, A. Varykhalov, I. V. Shvets, V. Y. Aristov, Continuous wafer-scale graphene on cubic-sic (001), Nano research 6 (8) (2013) 562–570.

[38] A. N. Chaika, O. V. Molodtsova, A. A. Zakharov, D. Marchenko, J. Sánchez-Barriga, A. Varykhalov, S. V. Babenkov, M. Portail, M. Zielinski, B. E. Murphy, S. A. Krasnikov, O. Lübben, I. V. Shvets, V. Y. Aristov, Rotated domain network in graphene on cubic-SiC(001), Nanotechnology 25 (13) (2014) 135605. doi:10.1088/0957-4484/25/13/135605.

[39] H.-C. Wu, A. N. Chaika, T.-W. Huang, A. Syrlybekov, M. Abid, V. Y. Aristov, O. V. Molodtsova, S. V. Babenkov, D. Marchenko, J. Sánchez-Barriga, P. S. Mandal, A. Y. Varykhalov, Y. Niu, B. E. Murphy, S. A. Krasnikov, O. Lübben, J. J. Wang, H. Liu, L. Yang, H. Zhang, M. Abid, Y. T. Janabi, S. N. Molotkov, C.-R. Chang, I. Shvets, Transport gap opening and high on–off current ratio in trilayer graphene with self-aligned nanodomain boundaries, ACS Nano 9 (9) (2015) 8967–8975. doi:10.1021/acsnano.5b02877.

[40] H.-C. Wu, A. N. Chaika, M.-C. Hsu, T.-W. Huang, M. Abid, M. Abid, V. Y. Aristov, O. V. Molodtsova, S. V. Babenkov, Y. Niu, B. E. Murphy, S. A. Krasnikov, O. Lübben, H. Liu, B. S. Chun, Y. T. Janabi, S. N. Molotkov, I. V. Shvets, A. I. Lichtenstein, M. I. Katsnelson, C.-R. Chang, Large positive in-plane magnetoresistance induced by localized states at nanodomain boundaries in graphene, Nature communications 8 (2017) 14453.

[41] V. Y. Aristov, A. N. Chaika, O. V. Molodtsova, I. M. Aristova, D. V. Potorochin, Nanostructured graphene on $\beta$-sic/si(001): Atomic and electronic structures, magnetic and transport properties (brief review), JETP Letters 113 (3) (2021) 176–193. doi:10.1134/s0021364021030036.
URL https://doi.org/10.1134/s0021364021030036

[42] S. Fedoseenko, D. Vyalikh, I. Iossifov, R. Follath, S. Gorovikov, R. Püttner, J.-S. Schmidt, S. Molodtsov, V. Adamchuk, W. Gudat, G. Kaindl, Commissioning results and performance of the high-resolution russian–german beamline at BESSY II, Nuclear Instruments and Methods in Physics Research Section A: Accelerators, Spectrometers, Detectors and Associated Equipment 505 (3) (2003) 718–728. doi:10.1016/s0168-9002(03)00624-7.

URL https://doi.org/10.1016/s0168-9002(03)00624-7

[43] S. L. Molodtsov, S. I. Fedoseenko, D. V. Vyalikh, I. E. Iossifov, R. Follath, S. A. Gorovikov, M. M. Brzhezinskaya, Y. S. Dedkov, R. Püttner, J.-S. Schmidt, V. K. Adamchuk, W. Gudat, G. Kaindl, High-resolution russian–german beamline at BESSY, Applied Physics A 94 (3) (2008) 501–505. doi:10.1007/s00339-008-4916-1.
URL https://doi.org/10.1007/s00339-008-4916-1

[44] J. Viefhaus, F. Scholz, S. Deinert, L. Glaser, M. Ilchen, J. Seltmann, P. Walter, F. Siewert, The variable polarization XUV beamline p04 at PETRA III: Optics, mechanics and their performance, Nuclear Instruments and Methods in Physics Research Section A: Accelerators, Spectrometers, Detectors and Associated Equipment 710 (2013) 151–154. doi:10.1016/j.nima.2012.10.110.
URL https://doi.org/10.1016/j.nima.2012.10.110

[45] S. V. Babenkov, V. Y. Aristov, O. V. Molodtsova, K. Winkler, L. Glaser, I. Shevchuk, F. Scholz, J. Seltmann, J. Viefhaus, A new dynamic-XPS end-station for beamline p04 at PETRA III/DESY, Nuclear Instruments and Methods in Physics Research Section A: Accelerators, Spectrometers, Detectors and Associated Equipment 777 (2015) 189–193. doi:10.1016/j.nima.2014.12.065.
URL https://doi.org/10.1016/j.nima.2014.12.065

[46] S. Doniach, M. Sunjic, Many-electron singularity in x-ray photoemission and x-ray line spectra from metals, Journal of Physics C: Solid State Physics 3 (2) (1970) 285.

[47] D. A. Shirley, High-resolution x-ray photoemission spectrum of the valence bands of gold, Physical Review B 5 (12) (1972) 4709.

[48] M. Anthony, M. Seah, Xps: Energy calibration of electron spectrometers. 1—an absolute, traceable energy calibration and the provision of atomic reference line energies, Surface and interface analysis 6 (3) (1984) 95–106.

[49] A. Chaika, S. Nazin, V. Semenov, S. Bozhko, O. Lübben, S. Krasnikov, K. Radican, I. Shvets, Selecting the tip electron orbital for scanning tunneling microscopy imaging with sub-ångström lateral resolution, EPL (Europhysics Letters) 92 (4) (2010) 46003.

[50] A. Chaika, N. Orlova, V. Semenov, E. Y. Postnova, S. Krasnikov, M. Lazarev, S. Chekmazov, V. Y. Aristov, V. Glebovsky, S. Bozhko, I. Shvets, Fabrication of [001]-oriented tungsten tips for high resolution scanning tunneling microscopy, Scientific reports 4 (2014) 3742.

[51] P. Giannozzi, O. Andreussi, T. Brumme, O. Bunau, M. B. Nardelli, M. Calandra, R. Car, C. Cavazzoni, D. Ceresoli, M. Cococcioni, N. Colonna, I. Carnimeo, A. D. Corso, S. de Gironcoli, P. Delugas, R. A. DiStasio, A. Ferretti, A. Floris, G. Fratesi, G. Fugallo, R. Gebauer, U. Gerstmann, F. Giustino, T. Gorni, J. Jia, M. Kawamura, H.-Y. Ko, A. Kokalj, E. Küçükbenli, M. Lazzeri, M. Marsili, N. Marzari, F. Mauri, N. L. Nguyen, H.-V. Nguyen, A. O. de-la Roza, L. Paulatto, S. Poncé, D. Rocca, R. Sabatini, B. Santra, M. Schlipf, A. P. Seitsonen, A. Smogunov, I. Timrov, T. Thonhauser, P. Umari, N. Vast, X. Wu, S. Baroni, Advanced capabilities for materials modelling with quantum ESPRESSO, Journal of Physics: Condensed Matter 29 (46) (2017) 465901. doi:10.1088/1361-648x/aa8f79.
URL https://doi.org/10.1088/1361-648x/aa8f79

[52] K. F. Garrity, J. W. Bennett, K. M. Rabe, D. Vanderbilt, Pseudopotentials for high-throughput DFT calculations, Computational Materials Science 81 (2014) 446–452. doi:10.1016/j.commatsci.2013.08.053.
URL https://doi.org/10.1016/j.commatsci.2013.08.053

[53] J. P. Perdew, A. Zunger, Self-interaction correction to density-functional approximations for many-electron systems, Physical Review B 23 (10) (1981) 5048–5079. doi:10.1103/physrevb.23.5048.
URL https://doi.org/10.1103/physrevb.23.5048

[54] K. Zhussupbekov, K. Walshe, B. Walls, A. Ionov, S. I. Bozhko, A. Ksenz, R. N. Mozhchil, A. Zhussupbekova, K. Fleischer, S. Berman, I. Zhilyaev, D. D. O'Regan, I. V. Shvets, Surface modification and subsequent fermi density enhancement of bi(111), The Journal of Physical Chemistry C 125 (10) (2021) 5549–5558. doi:10.1021/acs.jpcc.0c07345.
URL https://doi.org/10.1021/acs.jpcc.0c07345

[55] A. Kokalj, Computer graphics and graphical user interfaces as tools in simulations of matter at the atomic scale, Computational Materials Science 28 (2) (2003) 155–168. doi:10.1016/s0927-0256(03)00104-6.
URL https://doi.org/10.1016/s0927-0256(03)00104-6

[56] P.-O. Löwdin, On the non-orthogonality problem connected with the use of atomic wave functions in the theory of molecules and crystals, The Journal of Chemical Physics 18 (3) (1950) 365–375. doi:10.1063/1.1747632.
URL https://doi.org/10.1063/1.1747632

[57] G. S. Szymański, T. Grzybek, H. Papp, Influence of nitrogen surface functionalities on the catalytic activity of activated carbon in low temperature SCR of NO with NH3, Catalysis Today 90 (1-2) (2004) 51–59. doi:10.1016/j.cattod.2004.04.008.
URL https://doi.org/10.1016/j.cattod.2004.04.008

[58] S. Kundu, W. Xia, W. Busser, M. Becker, D. A. Schmidt, M. Havenith, M. Muhler, The formation of nitrogen-containing functional groups on carbon nanotube surfaces: a quantitative XPS and TPD study, Physical Chemistry Chemical Physics 12 (17) (2010) 4351. doi:10.1039/b923651a.
URL https://doi.org/10.1039/b923651a

[59] K. Kousar, T. Ljungdahl, A. Wetzel, M. Dowhyj, H. Oskarsson, A. S. Walton, M. S. Walczak, R. Lindsay, An exemplar imidazoline surfactant for corrosion inhibitor studies: Synthesis, characterization, and physicochemical properties, Journal of Surfactants and Detergents 23 (1) (2019) 225–234. doi:10.1002/jsde.12363.
URL https://doi.org/10.1002/jsde.12363

[60] J.-P. Yang, H.-P. Hu, Z.-Y. Cheng, X.-J. Qiu, C.-X. Wang, Structural insights into the coordination and selective extraction of copper(II) by tertiary amine ligands derived from 2-aminomethylpyridine, Polyhedron 128 (2017) 76–84. doi:10.1016/j.poly.2017.02.037.
URL https://doi.org/10.1016/j.poly.2017.02.037

[61] J. Ederer, P. Janoš, P. Ecorchard, J. Tolasz, V. Štengl, H. Beneš, M. Perchacz, O. Pop-Georgievski, Determination of amino groups on functionalized graphene oxide for polyurethane nanomaterials: XPS quantitation vs. functional speciation, RSC Advances 7 (21) (2017) 12464–12473. doi:10.1039/c6ra28745j.
URL https://doi.org/10.1039/c6ra28745j

[62] N. Graf, E. Yegen, T. Gross, A. Lippitz, W. Weigel, S. Krakert, A. Terfort, W. E. Unger, XPS and NEXAFS studies of aliphatic and aromatic amine species on functionalized surfaces, Surface Science 603 (18) (2009) 2849–2860. doi:10.1016/j.susc.2009.07.029.
URL https://doi.org/10.1016/j.susc.2009.07.029

[63] P. Finn, W. L. Jolly, Nitrogen ls binding energies of some azide, dinitrogen, and nitride complexes of transition metals, Inorganic Chemistry 11 (6) (1972) 1434–1435. doi:10.1021/ic50112a056.
URL https://doi.org/10.1021/ic50112a056

[64] C. Agnès, J.-C. Arnault, F. Omnès, B. Jousselme, M. Billon, G. Bidan, P. Mailley, XPS study of ruthenium tris-bipyridine electrografted from diazonium salt derivative on microcrystalline boron doped diamond, Physical Chemistry Chemical Physics 11 (48) (2009) 11647. doi:10.1039/b912468c.
URL https://doi.org/10.1039/b912468c

[65] Y. Xu, M. G. Schwab, A. J. Strudwick, I. Hennig, X. Feng, Z. Wu, K. Müllen, Screen-printable thin film supercapacitor device utilizing graphene/polyaniline inks, Advanced Energy Materials 3 (8) (2013) 1035–1040. doi:10.1002/aenm.201300184.
URL https://doi.org/10.1002/aenm.201300184

[66] T. Lin, J. Chen, H. Bi, D. Wan, F. Huang, X. Xie, M. Jiang, Facile and economical exfoliation of graphite for mass production of high-quality graphene sheets, J. Mater. Chem. A 1 (3) (2013) 500–504. doi:10.1039/c2ta00518b.
URL https://doi.org/10.1039/c2ta00518b

[67] M. P. Seah, W. Dench, Quantitative electron spectroscopy of surfaces: A standard data base for electron inelastic mean free paths in solids, Surface and interface analysis 1 (1) (1979) 2–11.

[68] T. Okajima, K. Teramoto, R. Mitsumoto, H. Oji, Y. Yamamoto, I. Mori, H. Ishii, Y. Ouchi, K. Seki, Polarized nexafs spectroscopic studies of poly (butylene terephthalate), poly (ethylene terephthalate), and their model compounds, The Journal of Physical Chemistry A 102 (36) (1998) 7093–7099.

[69] D. De Oteyza, A. Sakko, A. El-Sayed, E. Goiri, L. Floreano, A. Cossaro, J. M. Garcia-Lastra, A. Rubio, J. Ortega, Inversed linear dichroism in f k-edge nexafs spectra of fluorinated planar aromatic molecules, Physical Review B 86 (7) (2012) 075469.

[70] A. V. Syugaev, A. N. Maratkanova, A. A. Shakov, N. V. Lyalina, D. A. Smirnov, Polyaniline films electrodeposited on iron from oxalic acid solution: spectroscopic analysis of chemical structure, Journal of Solid State

Electrochemistry 22 (10) (2018) 3171–3182. doi:10.1007/s10008-018-4033-9.
URL https://doi.org/10.1007/s10008-018-4033-9

[71] M. Magnuson, J.-H. Guo, S. M. Butorin, A. Agui, C. Såthe, J. Nordgren, A. P. Monkman, The electronic structure of polyaniline and doped phases studied by soft x-ray absorption and emission spectroscopies, The Journal of Chemical Physics 111 (10) (1999) 4756–4761. doi:10.1063/1.479238.
URL https://doi.org/10.1063/1.479238

[72] S. Yau, Y. Lee, C. Chang, L. Fan, Y. Yang, W.-P. Dow, Structures of aniline and polyaniline molecules adsorbed on au(111) electrode: as probed by in situ STM, ex situ XPS, and NEXAFS, The Journal of Physical Chemistry C 113 (31) (2009) 13758–13764. doi:10.1021/jp9027194.
URL https://doi.org/10.1021/jp9027194

[73] C. Kolczewski, R. Püttner, O. Plashkevych, H. Ågren, V. Staemmler, M. Martins, G. Snell, A. S. Schlachter, M. Sant'Anna, G. Kaindl, L. G. M. Pettersson, Detailed study of pyridine at the c 1s and n 1s ionization thresholds: The influence of the vibrational fine structure, The Journal of Chemical Physics 115 (14) (2001) 6426–6437. doi:10.1063/1.1397797.
URL https://doi.org/10.1063/1.1397797

[74] C. Hannay, D. Duflot, J.-P. Flament, M.-J. Hubin-Franskin, The core excitation of pyridine and pyridazine: An electron spectroscopy and ab initio study, The Journal of Chemical Physics 110 (12) (1999) 5600–5610. doi:10.1063/1.478458.
URL https://doi.org/10.1063/1.478458

[75] J. A. Horsley, J. Stöhr, A. P. Hitchcock, D. C. Newbury, A. L. Johnson, F. Sette, Resonances in the k shell excitation spectra of benzene and pyridine: Gas phase, solid, and chemisorbed states, The Journal of Chemical Physics 83 (12) (1985) 6099–6107. doi:10.1063/1.449601.
URL https://doi.org/10.1063/1.449601

[76] G. Liu, Y. Gan, R. Quhe, P. Lu, Strain dependent electronic and optical properties of PtS2 monolayer, Chemical Physics Letters 709 (2018) 65–70. doi:10.1016/j.cplett.2018.08.029.
URL https://doi.org/10.1016/j.cplett.2018.08.029

[77] K. Zhussupbekov, C. P. Cullen, A. Zhussupbekova, I. V. Shvets, G. S. Duesberg, N. McEvoy, C. Ó. Coileáin, Electronic and structural characterisation of polycrystalline platinum disulfide thin films, RSC Advances 10 (69) (2020) 42001–42007. doi:10.1039/d0ra07405e.
URL https://doi.org/10.1039/d0ra07405e